STRUCTURAL BIOLOGY

Dynamic allosteric communication pathway directing differential activation of the glucocorticoid receptor

C. Köhler[1], G. Carlström[2], A. Gunnarsson[3], U. Weininger[4], S. Tångefjord[1,3], V. Ullah[1], M. Lepistö[1], U. Karlsson[3], T. Papavoine[1], K. Edman[3]*, M. Akke[4]*

Allosteric communication within proteins is a hallmark of biochemical signaling, but the dynamic transmission pathways remain poorly characterized. We combined NMR spectroscopy and surface plasmon resonance to reveal these pathways and quantify their energetics in the glucocorticoid receptor, a transcriptional regulator controlling development, metabolism, and immune response. Our results delineate a dynamic communication network of residues linking the ligand-binding pocket to the activation function-2 interface, where helix 12, a switch for transcriptional activation, exhibits ligand- and coregulator-dependent dynamics coupled to graded activation. The allosteric free energy responds to variations in ligand structure: subtle changes gradually tune allostery while preserving the transmission pathway, whereas substitution of the entire pharmacophore leads to divergent allosteric control by apparently rewiring the communication network. Our results provide key insights that should aid in the design of mechanistically differentiated ligands.

INTRODUCTION

Molecular communication within and between proteins forms the basis for biological signaling. Allostery involves coupling of ligand binding at one site with a conformational or dynamic change at a distant site, thereby affecting binding at that site. Identifying the transmission pathways between sites and understanding their dynamic nature is of fundamental interest and potentially of high relevance for drug design, where distinct ligands may drive differentiating effects downstream of the signaling events. Here, we identify and explore the allosteric communication network within the glucocorticoid receptor (GR) ligand-binding domain (LBD).

GR is a nuclear hormone receptor with essential roles in metabolism and resolution of inflammation (*1*). GR agonists are efficacious for treatment of inflammatory, allergic, and immunological disorders (*2*, *3*), but it remains a longstanding challenge to design differentiating ligands that separate the anti-inflammatory efficacy from side effects such as diabetes, muscle wasting, and osteoporosis (*4*). GR comprises the N-terminal domain, the DNA binding domain, and the C-terminal LBD. Ligand-free GR predominantly resides in a chaperone complex in the cytoplasm. Ligand binding leads to partial release of chaperone proteins and nuclear translocation. Within the nucleus, GR binds to specific DNA sequences and promotes coregulator assembly and transcriptional regulation (*1*).

Ligands bind to the fully occluded binding pocket at the center of the LBD (Fig. 1A) (*5*–*7*) and modulate the structure of the receptor (*8*, *9*). The receptor conformation, in turn, directs the DNA interaction pattern and guides the protein composition of the enhancer or promotor complexes to drive a specific genomic response (*1*, *10*). Allosteric effects between the intrinsically disordered N-terminal domain and the DNA binding domain have been investigated in detail by Hilser and coworkers (*11*), showing how binding to individual domains shapes the ensemble of states and tunes the output between activation and repression. However, less is known about ligand-driven allosteric effects and how these might influence signaling.

The LBD harbors two regions involved in binding coregulator proteins: the activation function 2 (AF-2), located at the interface between helices 3, 4, and 12 (*1*, *5*), and the transcriptional activation function tau2, which has been mapped to helix 1 (*1*, *12*). Crystal structures of GR LBD in complex with different ligands and coregulator peptides have shown that the receptor can adopt different conformations (*5*–*7*, *9*). In particular, the position of helix 12 is of key importance for receptor activity across the nuclear hormone receptor family (*13*–*17*). Recent reports on one other nuclear hormone receptor, the peroxisome proliferator–activated receptor γ (PPARγ), have demonstrated that helix 12 and the coregulator-binding surface adopt an ensemble of conformations, the relative populations of which respond to ligand binding (*18*–*20*). This indicates that conformational flexibility forms an integral part of receptor activation and leads to the hypothesis that ligand-driven shifts within conformational ensembles explain how different ligands can promote different levels of receptor activation (graded response) and tissue-specific effects (biased signaling).

Recent developments in nuclear magnetic resonance (NMR) have made it possible to detect weakly populated conformational states and determine their lifetimes (*21*, *22*). High-resolution NMR studies of GR LBD have previously been hampered by poor spectrum quality and sample aggregation, but we recently reported near-complete backbone assignments for wild-type GR LBD (GR_{wt}) and the stabilized F602S mutant (GR_{F602S}) in the ligand- and coregulator-bound state (*23*). Building on that work, here we identify the structural pathways of allosteric transmission, including a dynamic coupling between the ligand-binding pocket and the coregulator interfaces AF-2 and tau2. We further describe how activation is manifested through the dynamic equilibrium of alternative helix 12 conformations and how this responds to binding various ligands and coregulator peptides. Combining NMR with surface plasmon resonance (SPR), we unravel the free energies of allostery between

[1]Respiratory, Inflammation and Autoimmunity, Pharmaceutical Sciences, R&D, AstraZeneca, Gothenburg, Sweden. [2]Centre for Analysis and Synthesis, Department of Chemistry, Lund University, P.O. Box 124, 221 00 Lund, Sweden. [3]Discovery Sciences, Pharmaceutical Sciences, R&D, AstraZeneca, Gothenburg, Sweden. [4]Division of Biophysical Chemistry, Center for Molecular Protein Science, Department of Chemistry, Lund University, P. O. Box 124, 221 00 Lund, Sweden.
*Corresponding author. Email: mikael.akke@bpc.lu.se (M.A.); karl.edman@astrazeneca.com (K.E.)

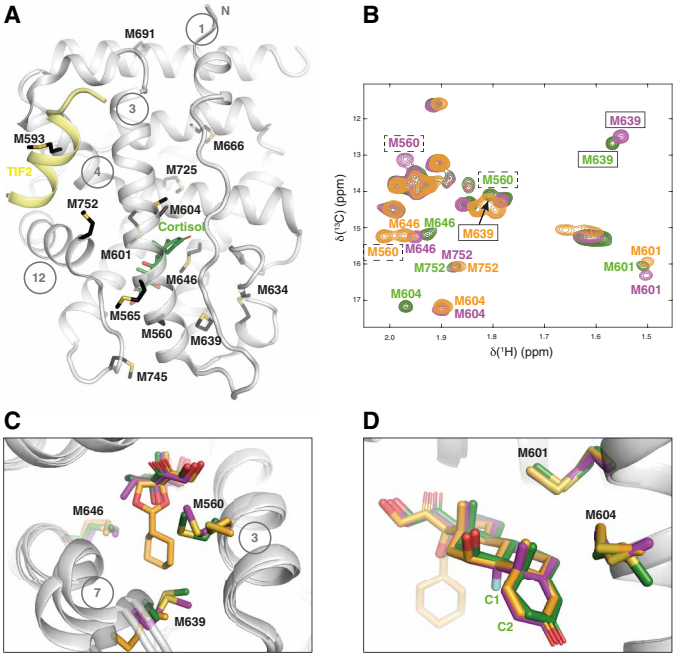

Fig. 1. Overview of the GR LBD structure and location of methionine residues. (**A**) Ribbon representation of the GR LBD (gray), with the side chains of the 13 methionine residues shown in stick representation (black with yellow sulfur). The ligand cortisol (green) binds in the ligand-binding pocket, and the TIF2 coactivator peptide (yellow) binds at the AF-2 site. (**B**) Comparison of the methionine methyl region of the ^{1}H-^{13}C HSQC spectra of three different GR_{wt}-ligand-TIF2 ternary complexes. The spectra are color-coded to indicate the bound ligand: cortisol (green), dex (magenta), and dibC (orange). Peaks annotated with residue number correspond to methionine side chains shown in (C) and (D). M560 and M639, which show the largest conformational changes, are highlighted with boxes (full or dashed). The minor chemical shift changes observed for M752 likely reflect changes in the relative populations of helix 12 conformational states (see table S1). (**C** and **D**) Close-up views of the ligand-binding pocket with the three ternary complexes superimposed showing the ligands and key methionine side chains in stick representation. Protein Data Bank (PDB) accession codes: GR-cortisol-TIF2, 4P6X (*47*); GR-dex-TIF2, 4UDC (*6*); GR-dibC-TIF2, 4UDD (*6*).

ligand-binding, coregulator-binding, and helix 12 activation and quantify the allosteric response to variations in coregulator identity and ligand structure. We demonstrate that the allosteric transmission pathway is preserved among ligands exhibiting subtle variations in structure, whereas different classes of ligands with distinct pharmacophores apparently rewire the allosteric transmission pathway, opening the possibility to design novel ligands that exert specific downstream effects.

RESULTS

Conformational dynamics link the ligand-binding pocket and AF-2 interface

To study the structural and dynamical consequences of ligand and coregulator binding to the LBD, we introduced $^{13}CHD_2$-labeled methyl groups in methionine residues, which have favorable NMR properties (*24*) and are distributed throughout the LBD, including the ligand-binding pocket and the AF-2 coregulator-binding site (Fig. 1A). The 13 LBD methionines have easily distinguishable methyl signals in the ^{1}H-^{13}C heteronuclear single-quantum coherence (HSQC) spectrum, which we assigned by site-specific methionine to leucine replacements (*23*). As shown in Fig. 1 (B to D), chemical shift changes of the methionine methyl groups sensitively report on structural and dynamical differences between various ligand complexes. For example, the cyclohexyl substituent of desisobutyryl-ciclesonide (dibC) extends into a region between helices 3 and 7 (Fig. 1C), where it pushes on M560 and M639, causing significant changes in the chemical shifts of these residues (Fig. 1B). In the same region, the methyl group in the C16 position of dexamethasone (dex) changes the environment of M560 relative to that in the cortisol-bound receptor, leading to further differences in the chemical shift for this residue among the different ligand-bound forms. In contrast, the ligands are relatively conserved at the other end of the ligand-binding pocket (Fig. 1D) and the chemical shift of M601 remains in a similar position for all three complexes. However, we note that the chemical shift of M604 is distinct for the complex with cortisol, which, unlike dex and dibC, lacks a conjugated double bond at the C1-C2 position (Fig. 1D). Last, compared to the methionines described above, the chemical shift of M752 shows only minor changes in response to the structural differences of the three ligands (Fig. 1B), in keeping with its remote location at the AF-2 interface (Fig. 1A). However, these subtle chemical shift changes provide critical information on gradual shifts in the relative populations of alternative helix 12 conformations, as explained further below.

We next investigated how these ligand-specific effects might translate into altered conformational dynamics of the LBD. We performed ^{13}C Carr-Purcell-Meiboom-Gill (CPMG) relaxation dispersion experiments (*24*) to directly monitor dynamic exchange between conformations in GR_{wt} and GR_{F602S}. Initially, we studied GR_{F602S} in complex with dex and a peptide from the TIF2 coregulator (GR_{F602S}-dex-TIF2). M752, located in the N-terminal part of helix 12 and interacting with the bound TIF2 peptide, shows a marked relaxation dispersion profile indicating exchange dynamics on the millisecond time scale between alternative conformations (Fig. 2A). The results are similar for GR_{wt}-dex-TIF2 (see Fig. 3A), but the data quality is higher for GR_{F602S}, presumably because of its greater stability and solubility (*5*). M565, located in helix 3 near helix 12, also shows relaxation dispersion in the GR_{F602S}-dex-TIF2 complex, albeit of much lower amplitude (Fig. 2A). Furthermore, M601, located in the ligand-binding pocket, also exhibits enhanced relaxation through line broadening, resulting in low signal intensity (Fig. 1B). Other methionine side chains do not show signs of conformational exchange. For example, there is no significant conformational exchange for M593, which is located in helix 4 and in contact with TIF2, suggesting that this part of the AF-2 motif adopts a single conformation in the GR-dex-TIF2 complex.

To probe further the conformational exchange dynamics, we performed backbone ^{15}N CPMG dispersion experiments (*21*, *25*) on GR_{wt} and GR_{F602S} in complex with dex and the TIF2 peptide. The relaxation data provide unequivocal evidence of conformational exchange in GR_{wt}-dex-TIF2, but broad NMR lines and poor signal-to-noise ratios leave few residues amenable to detailed analysis by CPMG experiments. The situation is improved for GR_{F602S}-dex-TIF2, which yielded significant relaxation dispersions for 14 residues (fig. S1). The backbone data reveal conformational exchange for several additional residues surrounding the methionines showing relaxation dispersion or line broadening (M752, M565, and M601; described above). Figure 2B highlights all residues exhibiting conformational exchange on the GR LBD structure. E751, L753, and

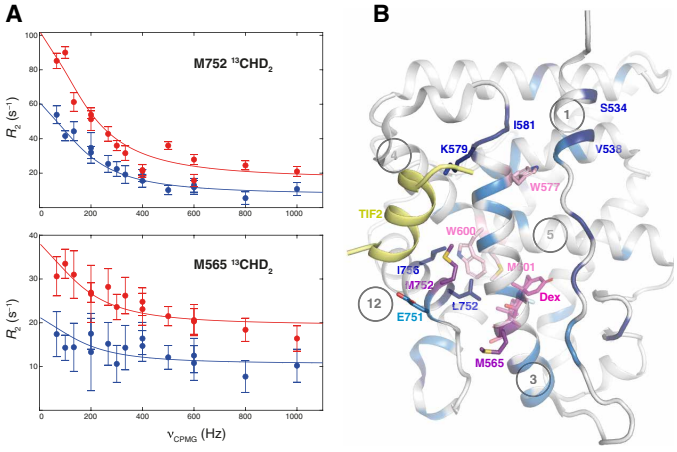

Fig. 2. Conformational exchange detected for the backbone and methionine side chains in GR LBD. (**A**) Side-chain ^{13}C CPMG relaxation dispersion data for M752 and M565 for GR$_{F602S}$-dex-TIF2. Blue and red symbols represent data acquired at static magnetic field strengths of 14.1 and 18.8 T, respectively. (**B**) Location of exchanging residues in GR LBD. Residues showing significant CPMG relaxation dispersion profiles are colored dark blue (^{15}N backbone data; fig. S1) or violet (^{13}C methionine methyl data), whereas nonquantifiable but exchange-broadened residues are colored light blue (^{15}N backbone) or pink (^{13}C methionine methyl, ^{15}N tryptophan indole). The exchanging backbone amides are located in helices 1, 3, 5, 7, 9, 11, and 12 and a loop proximal to helix 1. The exchanging side chains are M565, M601 and M752, and W577 and W600. PDB accession code for GR-dex-TIF2: 4UDC (*6*).

I756 in the N-terminal half of helix 12 exhibits conformational exchange, whereas the C-terminal half, which is more remote from the ligand-binding site and the bound peptide, is unaffected. E751 is in direct contact with the TIF2 peptide. I756, together with M752, forms part of the AF-2 pocket where the canonical LxxLL coregulator motif binds. L753, on the other hand, forms part of the ligand-binding pocket where it contacts W600 in helix 5. W600, in turn, is centrally placed and is adjacent to both M601 and I756. Both the indole amino group of W600 and the methyl of M601 exhibit weak exchange signals.

Together, the results reveal a tight network of dynamic interactions bridging from the ligand to the N-terminal end of helix 12 (Fig. 2B). This network delineates a pathway for dynamic allosteric communication between the ligand-binding pocket and the AF-2 interface.

Conformational dynamics link the coregulator-binding sites AF-2 and tau2

S534, V538, E542, and L544 in helix 1 all show ^{15}N relaxation dispersion (fig. S1) and belongs to the coregulator-binding site tau2 (residues 529 to 556). Several exchanging residues at the C-terminal end of helix 3 connect this segment to the AF-2 interface (Fig. 2B). A key residue for this pathway appears to be K579, which interacts directly with the TIF2 peptide and, together with E755, forms a charge clamp that orients the coregulator motif (*5*). Next to K579, residues A580 and I581 also exhibit ^{15}N relaxation dispersion. In addition, K576 and the side chain of W577 exhibit ^{15}N exchange broadening, one helix turn below. Together, these residues form a second pathway of dynamic coupling, linking AF-2 to tau2, which suggests that coregulator binding at one of the sites might allosterically affect the conformation of the other site and thereby its coregulator affinity. These results thus provide an atomic-resolution explanation for the previous observation that the tau2-binding coregulator Hic-5 acts to stabilize higher-order GR-coregulator complexes (*1*, *26*, *27*).

GR exhibits a rapid equilibrium between alternative conformations

To quantify the exchange dynamics, we fitted a minimal, two-state exchange process simultaneously to the ^{13}C and ^{15}N dispersion profiles of GR$_{F602S}$-dex-TIF2. The fitted parameters comprise the exchange rate, k_{ex} = 1147 ± 82 s^{-1}; the relative population of the minor (high-energy) state, p_m = 19 ± 7% (p_m = 1 − p_M, where p_M is the major ground state); and the residue-specific chemical shift differences between the exchanging conformational states, $\Delta\delta(^{15}N) = |\delta_m - \delta_M|$ = 0.5 to 1.2 parts per million (ppm) (fig. S2). Fitting the GR$_{wt}$-dex-TIF2 data with k_{ex} and p_m fixed to values similar to those obtained for GR$_{F602S}$-dex-TIF2 yields wild-type Δδ values in good agreement with the results for the mutant (fig. S2), strongly indicating that the exchanging conformations are highly similar in the two protein variants; this result is expected given the remote location of the site of mutation from the AF-2 site.

The present finding that the N-terminal end of helix 12 undergoes dynamic exchange between alternative conformations in the ternary complex goes beyond previous observations from crystal structures of GR, where the helix conformation varies among different ligand- and coregulator-bound complexes. Because helix 12 forms a substantial part of the AF-2 surface, the alternative conformations can likely be distinguished by additional coregulator proteins and trigger downstream rearrangements leading to differential transcriptional activity. To this extent, the alternative conformations detected here might exhibit different levels of activation. On the basis of these observations, we formed the hypothesis that dynamic exchange between alternative conformations and their relative populations constitute a continuous dial for transcriptional activation that is tuned by the detailed structure of each individual ligand.

The dynamic equilibrium of helix 12 conformations responds to ligand and coregulator

To test this hypothesis, we next compared the ^{13}C CPMG relaxation dispersion results for M752 of GR$_{wt}$ in complex with five different steroid ligands [dex, cortisol, prednisolone (pred), AZ938, and dibC; Fig. 3] and two peptide fragments from the coregulator proteins TIF2 and PRGC1. The different GR$_{wt}$-ligand-TIF2 complexes show subtle variation in their dispersion profiles (Fig. 3, left), indicating that the bound ligands affect the exchange dynamics of M752, to gradually shift the relative populations of helix 12 conformations. The limited data, with M752 being the single probe, are not sufficiently precise to unequivocally quantify differences among these complexes in their exchange parameters. However, assuming that the exchanging helix 12 conformations—and, consequently, the ^{13}C chemical shift difference between them—are identical in all complexes, the magnitude of the dispersion step (i.e., the difference between the highest and lowest relaxation rates) in Fig. 3 should increase with the value of p_m. Thus, it appears that the complexes with cortisol, AZ938, and dibC (Fig. 3, B, D, and E) have lower p_m values than those with dex and pred (Fig. 3, A and C). This conclusion is also supported by the ^{13}C chemical shifts observed for M752 in the ^{1}H-^{13}C HSQC spectra of the GR$_{wt}$-ligand-TIF2 complexes (Fig. 1B), which scale as expected with p_m ($\delta_{obs} = \Delta\delta\, p_m + \delta_M$; table S1). Similar to our observations, changes in the relative populations of alternative receptor conformations were recently observed in a study using a chemical probe attached to helix 12 of PPARγ (*18*, *19*).

Upon substituting the TIF2 peptide for a PRGC1 peptide in the GR$_{wt}$-ligand-coregulator complexes, we observe that M752 no longer

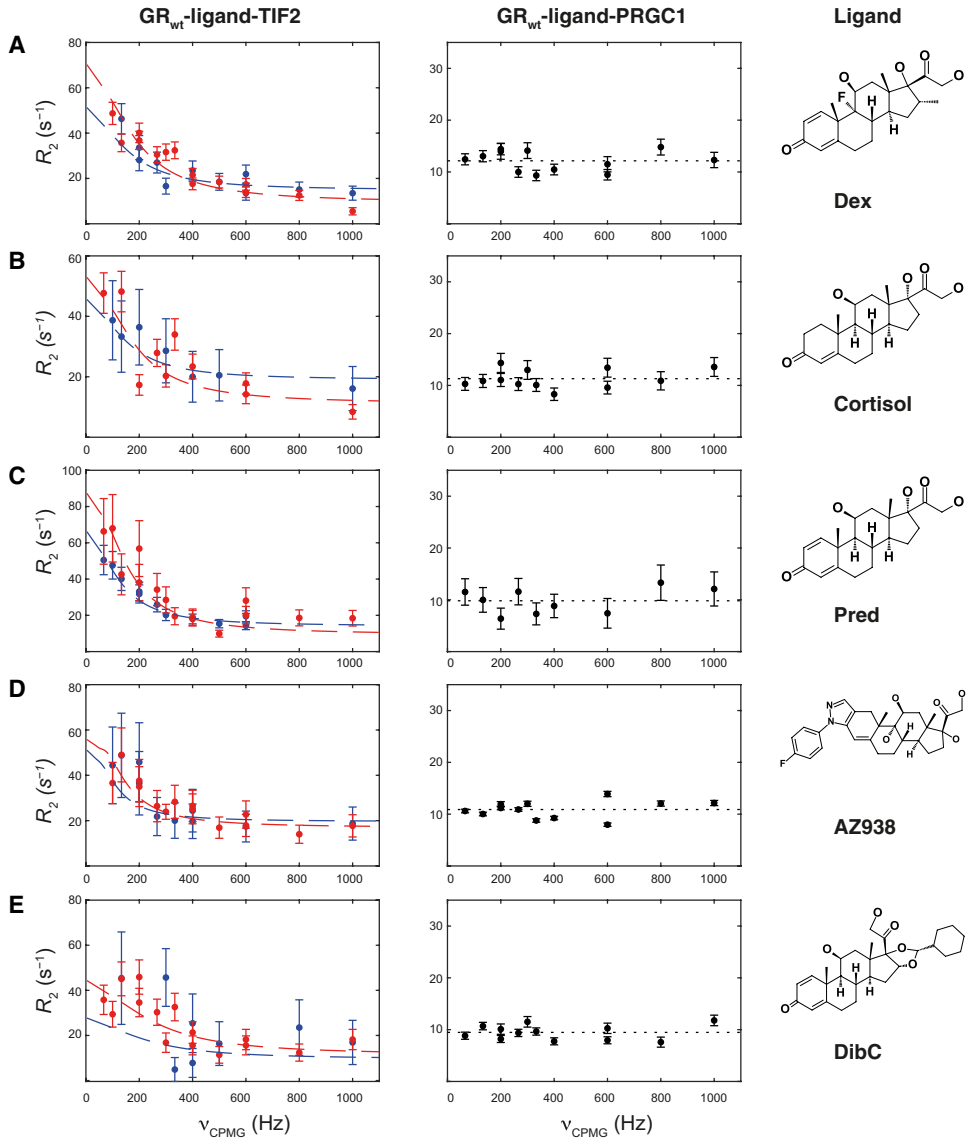

Fig. 3. Methyl ^{13}C CPMG relaxation dispersion data for residue M752. Data for five different GR$_{wt}$-ligand-TIF2 (left) and GR$_{wt}$-ligand-PRGC1 (right) complexes. The ligand structures are indicated to the right of the panels showing CPMG dispersion data: (**A**) dex, (**B**) cortisol, (**C**) pred, (**D**) cortivazol analog (AZ938), and (**E**) dibC. In fitting exchange parameters for the different complexes, we fixed $\Delta\delta_{CPMG}$ for M752 to the value obtained from the global fit for GR$_{F602S}$-dex-TIF2. Data for GR$_{wt}$-ligand-TIF2 were acquired at static magnetic field strengths of 14.1 T (blue) and 20.0 T (red). Data for GR$_{wt}$-ligand-PRGC1 were acquired at a static magnetic field strength of 18.8 T.

shows relaxation dispersion (Fig. 3), suggesting that a single conformation of helix 12 dominates in all of the GR$_{wt}$-ligand-PRGC1 complexes or possibly that the chemical shift is identical in the major and minor conformations. However, the former interpretation is supported by the result that M565 also does not show any dispersion in GR$_{wt}$-dex-PRGC1, contrary to the case in the TIF2 complex (Fig. 2A). These data indicate that different coregulators with unique amino acid sequences vary in their ability to drive ligand-specific responses and that the thermodynamic coupling is distinct (see further below).

Agonist efficacy in functional assays follows the population of helix 12 minor conformation

To investigate whether the observed population shift of helix 12 conformations might correlate with the functional response of GR, we measured agonist efficacy in a transactivation reporter gene assay (Fig. 4) (*28*). The top effect relative to dex (100%) varies from 77% for dibC and cortisol, 86% for pred, to 90% for AZ938. Despite being a partial agonist, dibC binds GR with high potency. Conversely, dex and pred have relatively high efficacies but weaker potencies for GR. These results underscore that efficacy does not directly relate to potency. However, the functional efficacy matches qualitatively with the p_m values from the NMR relaxation experiments, where the GR$_{wt}$ complexes with dibC and cortisol both appear to have lower p_m than the compounds with higher efficacy. The cortivazol analog AZ938 forms a notable exception with high functional efficacy combined with a low p_m value. AZ938 is distinct from the other steroid ligands in that the A-ring keto-moiety has been replaced with a fluorophenyl diazole (Fig. 3D). Structural studies have shown

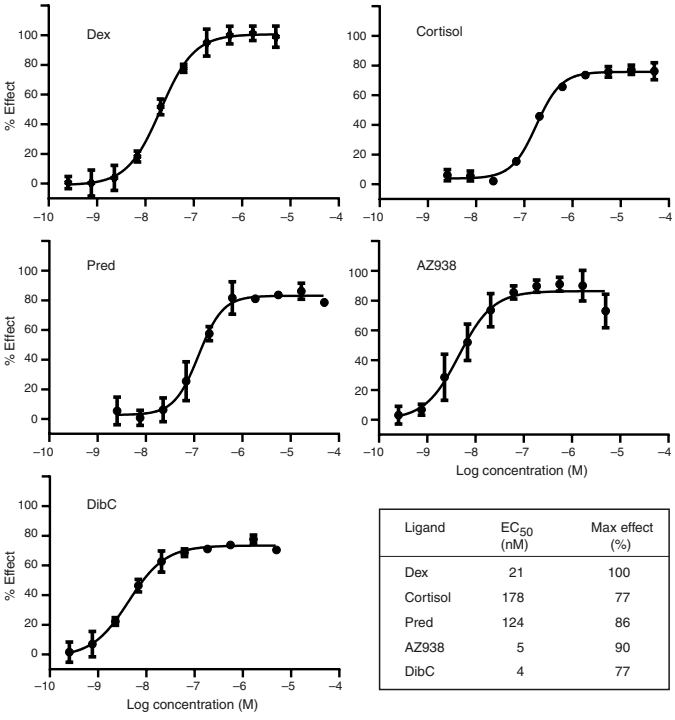

Ligand	EC_{50} (nM)	Max effect (%)
Dex	21	100
Cortisol	178	77
Pred	124	86
AZ938	5	90
DibC	4	77

Fig. 4. GR reporter gene assay data. Agonist activity at the human GR monitored in a GRE-*lacZ*–transfected ChagGo-K-1 cell-based reporter assay. The induction of *lacZ* gene expression through the binding of ligand-bound GR to the glucocorticoid response element in the promoter of *lacZ* is measured as the up-regulation of the β-galactosidase activity through a change in absorbance. The assay was run on at least three separate occasions for each ligand. See Materials and Methods for details.

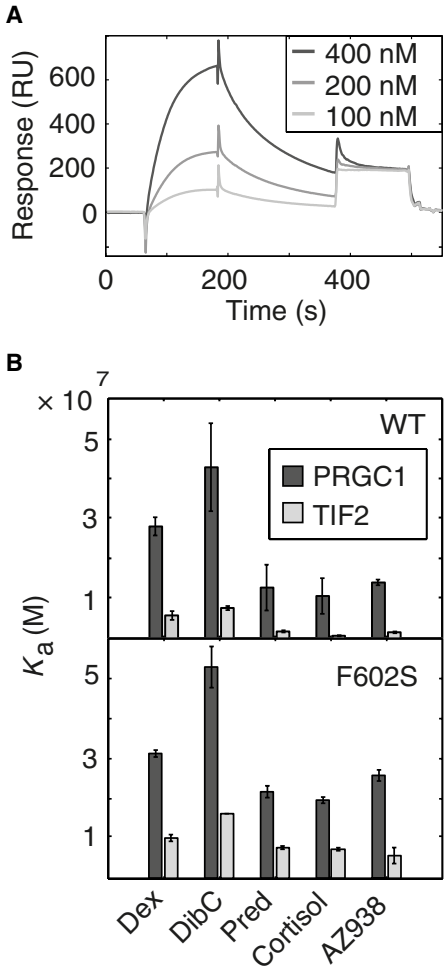

Fig. 5. SFR experiments characterizing coregulator-binding affinities to various GR-ligand complexes. (**A**) Representative sensorgrams showing the SPR response upon binding versus time. (**B**) Histograms showing the variation in K_a of coregulator peptide binding to the ligand complexes of GR_{wt} and GR_{F602S}. The error bars indicate 1 SD ($n = 3$). Table S2 lists the SPR results in detail, including k_{off}, k_{on}, and error estimates, and fig. S3 shows the corresponding histograms.

that this motif induces a sizeable rearrangement of the ligand binding site, specifically affecting the conformations of Q570 and R611 such that a new pocket opens up between helices 3 and 5 (*29*). These structural changes may alter the allosteric communication pathway to the AF-2 site and affect the active helix 12 conformation, as also suggested by the chemical shift of M752 (table S1). On the basis of the results for the remaining four congeneric steroid ligands, we suggest that the minor conformation of helix 12 might represent the active receptor, in keeping with the hypothesis formulated above.

Coregulator-binding affinities show significant variation among ligand-LBD complexes

To get insights into the thermodynamic coupling between ligand and coregulator binding to GR-LBD, we used SPR to measure the kinetic on- and off-rate constants, k_{on} and k_{off}, which yield the equilibrium association constant, $K_a = k_{on}/k_{off}$. We measured these parameters for both PRGC1 and TIF2 peptide binding to the five different GR-ligand complexes, using both GR_{wt} and GR_{F602S} (Fig. 5 and fig. S3). The results show that k_{on}, k_{off}, and K_a vary among the different complexes. The kinetic rate constants determined by SPR also indicate that the off-rates of the coregulator peptides are too slow to give rise to the NMR relaxation dispersion profiles, thereby providing independent evidence that the latter are caused by conformational exchange within the ligand- and coregulator-bound states rather than exchange between free and bound states.

In comparing K_a among the different ligand-coactivator pairs, we find that both GR constructs have higher affinity for PRGC1 than for TIF2, irrespective of which ligand is bound. In addition, GR_{F602S} exhibits higher affinities than GR_{wt} in every case (table S2). The variation in K_a among the different GR-ligand complexes tends to be greater for TIF2 than for PRGC1. Furthermore, the variation is greater in GR_{wt} than in GR_{F602S} for both coregulators.

Ligand structure tunes the allosteric free energy and can affect the transmission pathway

Allosteric coupling between the ligand- and coregulator-binding sites has been observed previously for several nuclear hormone receptors (*8*, *30*, *31*) but has rarely been quantified. To interpret in a unified and quantitative manner the combined experimental results from SPR and NMR in terms of allosteric couplings, we used a three-site statistical thermodynamic model for ligand (L) and coregulator (P) binding and transcriptional regulation (A) involving the conformational change of helix 12. This model involves three states for each site, corresponding to two unbound states, which are either binding incompetent or binding competent, and the bound state. To interpret

the present data, it suffices to include only a subset of all possible states (Fig. 6A; see fig. S4 and Supplementary Text for a full description of the model). The probability of each state is a function of the free energies of forming the binding-competent conformation at a given site (ΔG_i), binding to a site (Δg_{bi}), and allosteric coupling or cooperativity (Δg_{ij}) between sites (*32*–*34*). It has been shown that changes in allosteric effects can arise from population shifts within the ensemble of states as a consequence of changes in ΔG_i without any changes in Δg_{ij} (*34*). Here, we focus on isolating the free energies of site-to-site couplings, Δg_{ij}.

It is informative to calculate the ratio of binding affinities for pairs of different ternary complexes, because it reveals how allosteric couplings between sites vary with ligand and coregulator peptide identity. The free energy of binding a coregulator peptide to a GR-ligand complex is given by $\Delta G = \Delta G_P + \Delta g_{LP} + \Delta g_{LA} + \Delta g_{bP}$. It follows that the difference in ΔG between two different GR-ligand complexes is $\Delta\Delta G = -RT \ln[K_a(L_m, P_i)/K_a(L_n, P_i)] = \Delta\Delta g_{LP} + \Delta\Delta g_{LA}$. However, the minor variation in p_m (i.e., the relative population of active helix 12 conformations detected by NMR) between the different ternary complexes indicates that the variation $\Delta\Delta g_{LA}$ contributes relatively little to variations in coregulator-binding affinity (fig. S5), which instead is dominated by $\Delta\Delta g_{LP}$. Thus, the SPR results can be interpreted to extract differences between ligands in their strength of allosteric coupling to coregulator binding, $\Delta\Delta g_{LP}$.

Comparing complexes with different ligands but the same coregulator, the affinity ratios $K_a(L_m,P_i)/K_a(L_n,P_i)$ cover the range 2.3 to 11.7 for GR_{wt}-ligand-TIF2 and 1.2 to 4.0 for GR_{wt}-ligand-PRGC1 (table S2) when using as reference the GR_{wt}-cortisol-coregulator complex, which has the weakest affinity in both cases. Figure 6B shows a comparison of the relative allosteric coupling between the L and P sites, $\Delta\Delta g_{LP}$, for TIF2 and PRGC1 across the series of five ligands. The cooperativity Δg_{LP} varies significantly (by factors of 2 to 3) with the identity of both ligand and coregulator, although the standard errors are relatively large for PRGC1. Nonetheless, the datasets for the two coregulators are significantly correlated. This result suggests that the mechanism of allosteric transmission between the ligand-binding pocket and the AF-2 interface is highly related for the two coregulators.

GR_{F602S} shows higher affinity for coregulators, compared to GR_{wt} (Fig. 5 and fig. S3), but in this case, the ratios $K_a(L_m,P_i)/K_a(L_n,P_i)$ are considerably lower for both TIF2 and PRGC1, with the maximum ratio being less than 3 (table S2). This result is explained by stabilization of the binding-competent conformation of site P, $\Delta G_P(GR_{F602S}) < \Delta G_P(GR_{wt})$ (see fig. S5), in agreement with previous observations that the F602S mutation increases hormone responsiveness (*8*, *35*). However, the mutation does not seem to have any greater impact on the cooperativities between sites, Δg_{LP} or Δg_{PA} (fig. S5). Figure 6C shows the relative allostery, $\Delta\Delta g_{LP}$, in GR_{F602S}, which can be directly compared with the corresponding data for GR_{wt} (Fig. 6B). The data for the four complexes with ligands containing the cyclic ketone moiety (cortisol, pred, dex, and dibC) are highly correlated and fall on a straight line. This result reinforces the notion that for congeneric ligands, coregulator binding involves the same allosteric pathway between the ligand pocket and the AF-2 interface irrespective of the coregulator identity. Furthermore, the rank order among these complexes is preserved between GR_{wt} and GR_{F602S}, indicating that this conclusion holds for both protein variants, as also indicated by the CPMG relaxation dispersion data (Fig. 2 and fig. S2). The divergent result for AZ938 is likely because of its distinct structure, which results in conformational rearrangements in the AZ938 complex (described above) and apparently leads to a modified communication pathway from the ligand-binding pocket to the AF-2 site and an alternative helix 12 conformation (table S1). The results presented in Fig. 6 (B and C) thus reveal how these ligand-induced perturbations affect the free energy of allosteric coupling, Δg_{LP}.

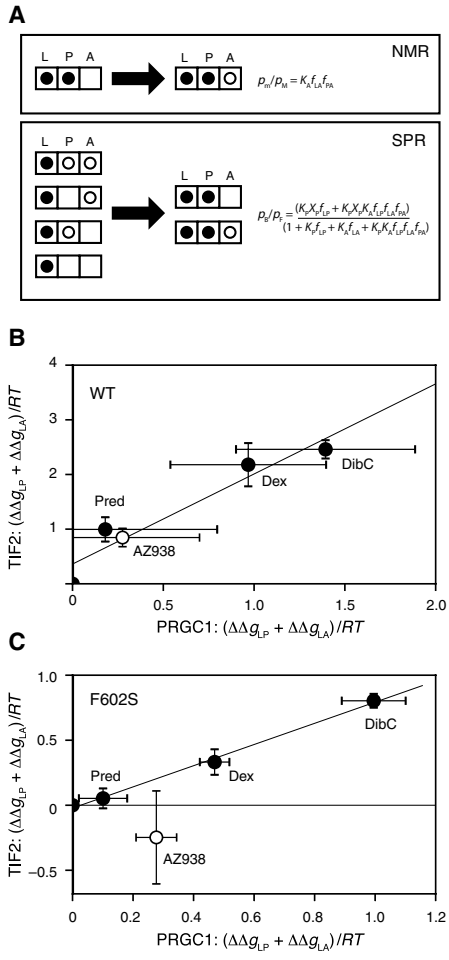

Fig. 6. Allosteric coupling between sites in GR LBD. (**A**) Statistical thermodynamic model of ligand and coregulator binding and activation of GR LBD relating to the current experimental results (see fig. S4 for the full model). The model includes three sites: the ligand-binding site, L; the coregulator-binding site, P; and transcriptional activation, A. Filled circles indicate bound sites; empty circles indicate unbound but binding-competent sites; boxes without circles indicate binding-incompetent sites. Top: NMR measures the population ratio between minor (inactive) and major (active) states, p_m/p_M. Bottom: SPR measures the population ratio of bound and free states: p_B/p_F. $K_i = \exp(-\Delta G_i/RT)$, $f_{ij} = \exp(-\Delta g_{ij}/RT)$, $X_P = \exp(-\Delta g_{bi}/RT)$ [C]. ΔG_i, free energy of forming a binding-competent site; Δg_{ij}, cooperativity between sites *i* and *j*; Δg_{bi}, free energy of coregulator binding to competent site; [C], concentration of free coregulator. (**B**) Covariance plot showing the relative free energy of cooperativity for TIF2 or PRGC1 binding to different GR_{wt}-ligand complexes, referenced to the GR_{wt}-cortisol complex: $\Delta\Delta g_{LP}$ + a minor contribution from $\Delta\Delta g_{LA}$. Empty circle, data involving AZ938; filled circles, data involving the four congeneric ligands. Error bars: 1 SD (table S3). Straight lines: Best-fit linear regression, excluding AZ938. Weighted Pearson's correlation coefficient $R = 0.98$ with 95% confidence interval (0.41 to 0.99). (**C**) Data as in (B), but for GR_{F602S}. $R = 0.998$ (0.919 to 0.999). The confidence interval of *R* was estimated using 10,000 Monte Carlo samples drawn from a binormal distribution, with widths taken from the experimental SDs (*46*).

Differential allosteric coupling of helix 12 activation with ligand or coregulator binding

On the basis of the results from the CPMG relaxation dispersion experiments and the functional assay, we tentatively interpret the major and minor conformations of helix 12 as transcriptionally "inactive" and "active," respectively, in line with conclusions reached for PPARγ (*18*–*20*). In the framework of the statistical thermodynamic model, the population ratio p_m/p_M depends on ΔG_A, Δg_{LA}, and Δg_{PA}, but the variation in p_m/p_M among GR_{wt}-ligand-TIF2 complexes depends only on Δg_{LA}. Thus, the NMR experiments probe the relative allosteric effect on the transcriptionally active conformation elicited by different ligands. Qualitatively, the NMR data show that Δg_{LA} depends on the ligand identity in the GR_{wt}-ligand-TIF2 complexes (Fig. 3), similar to our conclusions regarding Δg_{LP}. A semiquantitative interpretation indicates that p_m/p_M varies between 0.1 for dibC and cortisol to 0.2 for dex and pred, which corresponds to $\Delta\Delta g_{LA} \leq 0.7\ RT$ (fig. S7). Therefore, while the GR-dibC complex has the highest affinity for coregulator peptides and exerts the greatest cooperativity between the ligand- and peptide-binding sites, Δg_{LP} (Fig. 6, B and C), it displays weaker cooperativity between ligand binding and receptor activation, Δg_{LA}.

Next, comparing differences in p_m/p_M between TIF2- and PRGC1-bound ternary complexes, we isolate Δg_{PA}. The lack of detectable conformational exchange in the GR_{wt}-ligand-PRGC1 complexes (Fig. 3) suggests that a single conformation dominates in this case, indicating that PRGC1 shows either much stronger or weaker allostery, Δg_{PA}, compared to TIF2. Calculations suggest that PRGC1 has a stronger cooperativity Δg_{PA} than TIF2 by a factor of at least 2.5 (fig. S8); this result is similar to what is found for Δg_{LP}, as discussed above (fig. S6). In the GR_{wt}-ligand-PRGC1 complexes, any ligand-dependent variation in Δg_{LA} is unobservable because of the high level of activation. The marked difference between TIF2- and PRGC1-bound GR-LBD in their conformational dynamics highlights how the specific amino acid sequence of the coregulator can modulate the receptor's response to ligand binding and thereby affect downstream pathways.

DISCUSSION

Our results provide a unique view of the allosteric transmission pathway through which ligands modify the conformational dynamics of the receptor. While recognizing that NMR chemical shifts do not necessarily respond to conformational changes, potentially leaving "blind" spots in our analysis, we believe that uniform ^{15}N labeling provides a sufficient number of probes to offer a satisfactory view of exchange dynamics throughout the LBD. The CPMG relaxation dispersion data directly visualize a network of residues undergoing concerted dynamics that couples the ligand-binding site to the AF-2 and tau2 sites and helix 12 activation. Residues in the binding pocket connect the ligand to the N-terminal end of helix 12 and the C-terminal end of helix 3 and onward to helix 1, providing the means for the receptor to tailor the coregulator interactions in response to the ligand pharmacophore. The network identified here shows partial agreement with previous predictions derived from a statistical analysis of coevolution across the nuclear hormone receptor family (*36*) but differs in several respects from conclusions reached from mutagenesis and modeling studies (*8*, *37*) in that our data reveal a contiguous network that does not seem to include helix 11 as the primary conduit of communication. It is possible that these differences reflect the detailed variation in structural homology among nuclear hormone receptors.

We used the conformational dynamics of the M752 methyl group as the principal indicator of receptor activation in 10 different ternary complexes. While the use of a single probe limits the quantitative interpretation of the dynamic data alone, the full picture emerging from the combination of ^{13}C relaxation dispersion and chemical shift data, SPR, functional assays, and statistical thermodynamic modeling is consistent. Receptor activation is strongly dependent on the coregulator identity, and our model reveals how this, in turn, arises from ligand- and coregulator-dependent cooperativity between sites. Because coregulator expression profiles vary among cell types, this result indicates that the potential to achieve ligand-specific effects will vary between different tissues.

The mechanistic and quantitative model presented here describes how binding of various ligands and coregulators differentially affect receptor allostery to shift the dynamic ensemble between alternative conformations with different regulatory properties. Our results complement previous reports on allostery between the N-terminal domain and the DNA binding domain of GR, which have revealed how allostery varies among isoforms or mutational variants that destabilize individual domains and generate population shifts within the ensemble, leading to either activation or repression of transcription (*11*). The observed variation in the population of active conformations amount to regulation by a continuous dial rather than a binary structural switch, a phenomenon explaining key concepts such as graded response and biased signaling.

Our work further shows that the allosteric pathway is maintained for a given class of ligands with common pharmacophore, although subtle changes in ligand structure lead to variation in the allosteric free energy. By contrast, substantial changes in ligand structure can affect the interaction network within the protein, thereby rewiring the allosteric transmission pathway. Thus, ligands with different chemical scaffolds and pharmacophores may create new opportunities to influence the structural ensembles and communication pathways in unique ways that will be important to consider when developing mechanistically differentiating GR ligands (*3*, *13*, *17*, *28*, *38*).

MATERIALS AND METHODS

Expression and purification GR LBD

Construct design, expression, and purification of wild-type GR LBD (residues T529 to K777) and the mutant F602S were carried out as described (*23*). Expression of samples labeled with $^{12}C^{\beta}D_2{}^{12}C^{\gamma}D_2{}^{13}CHD_2$ methionine (*24*), synthesized in-house as described below, was carried out using the PASM-5052 autoinduction medium (*39*).

Synthesis of $^{12}C^{\beta}D_2{}^{12}C^{\gamma}D_2{}^{13}CHD_2$ methionine

(S)-2-(tert-Butoxycarbonylamino)-4-(((R)-3-(tert-butoxycarbonylamino)-3-(1,1,2,2 $^2H_4$)-carboxypropyl)disulfanyl)-(3,3,4,4,$^2H_4$)-butanoic acid

DL-Homocystine-(3,3,3′3′,4,4,4′4′$^2H_8$) (1.00 g, 3.62 mmol) was dissolved in 10% sodium carbonate (24.0 ml) and dioxane (21.0 ml) at 0°C. Di-*tert*-butyl dicarbonate (1.74 g, 7.96 mmol) was added portionwise, and the reaction mixture was allowed to reach room temperature and stirred for 18 hours. The pH was adjusted to 4 with 10% citric acid and extracted with ethyl acetate (3 × 50.0 ml). The organic layers were combined, dried ($MgSO_4$), and concentrated

under reduced pressure. This resulted in 1.72 g (quantitative yield) (*S*)-2-(*tert*-butoxycarbonylamino)-4-(((*R*)-3-(*tert*-butoxycarbonylamino)-3-(1,1,2,2,$^2H_4$)-carboxypropyl)disulfanyl)-(3,3,4,4, $^2H_4$)-butanoic acid as a white solid. [500 MHz, dimethyl sulfoxide (DMSO)] δ 1.38 (18 H, s), 3.98 (2 H, d), 7.15 (2 H, d), and 12.55 (2 H, bs). Liquid chromatography–mass spectrometry (LC-MS): mass/charge ratio (*m*/*z*) 477 $[M+H]^+$.

2-(tert-Butoxycarbonylamino)-4-(^{13}C, $^2H_2$)-(methylthio)-(3,3,4,4, $^2H_4$)-butanoic acid

(*S*)-2-(*tert*-Butoxycarbonylamino)-4-(((*R*)-3-(*tert*-butoxycarbonylamino)-3-(1,1,2,2,$^2H_4$)-carboxypropyl)disulfanyl)-(3,3,4,4,$^2H_4$)-butanoic acid (1.52 g, 3.20 mmol) was dissolved in 7% ammonium bicarbonate (12.0 ml) and DMSO (4.00 ml). The mixture was degassed, and (2*S*,3*S*)-1,4-dimercaptobutane-2,3-diol (0.540 g, 3.52 mmol) was added under inert atmosphere. The reaction was stirred at room temperature for 0.5 hours. Iodomethane-(^{13}C, $^2H_2$) (0.800 ml, 12.8 mmol) was added dropwise, and the reaction mixture was stirred for 2.5 hours. Dichloromethane (25.0 ml) was added to the reaction, and the organic layer was washed twice with 0.5 M hydrochloric acid (20.0 ml). The organic phase was dried ($MgSO_4$) and concentrated under reduced pressure. The compound was purified by preparative high-performance liquid chromatography (HPLC) on a Kromasil C8 column [10 μm 250 × 50 inside diameter (ID) mm] using a gradient of 15 to 55% acetonitrile in water/acetonitrile/formic acid 95/5/0.2 buffer over 25 min with a flow of 100 ml/min and detection by ultraviolet at 210 nm. This resulted in 0.370 g (45%) of 2-(*tert*-butoxycarbonylamino)-4-(^{13}C,$^2H_2$)-(methylthio)-(3,3,4,4,$^2H_4$)-butanoic acid as a white solid. (500 MHz, DMSO) δ 1.38 (9 H, s), 1.99 (1 H, d), 3.98 (1 H, d), 7.11 (1 H, d), and 12.48 (1 H, bs). LC-MS: *m*/*z* 255 $[M-H]^-$.

2-amino-4-(^{13}C, $^2H_2$)-(methylthio)-(3,3,4,4,$^2H_4$)-butanoic acid TFA salt

2-(*tert*-Butoxycarbonylamino)-4-(^{13}C,$^2H_2$)-(methylthio)-(3,3,4,4,$^2H_4$)-butanoic acid (0.340 g, 1.31 mmol) was dissolved in dichloromethane (1.00 ml) in a 25.0-ml flask. 2,2,2-Trifluoroacetic acid (TFA) (0.800 ml, 10.8 mmol) was added dropwise to the mixture at room temperature under inert atmosphere. The reaction was stirred for 2 hours. Water (4.00 ml) was added to the mixture and lyophilized, which was repeated two times, and resulted in 0.210 g (41%) of 2-amino-4-(^{13}C, $^2H_2$)-(methylthio)-(3,3,4,4,$^2H_4$)-butanoic acid as a TFA salt and a clear oil that solidified over time. (500 MHz, DMSO) δ 2.01 (1H, d), 3.99 (1 H, s), and 8.27 (2 H, bs).

NMR sample preparation

The protein was transferred at low concentration (<0.03 mM) to a 20 mM phosphate buffer [10% (v/v) D_2O] (pH 7.5) supplemented with 1% CHAPS, 2 mM dithiothreitol (DTT), 50 μM dex, 0.02% NaN_3, and protease inhibitor using a PD10 desalting column (GE Healthcare). After adding a suitable coactivator peptide, corresponding to a fragment of nuclear receptor coactivator 2 (KENALLRYLLDKDD; TIF2) or peroxisome proliferator–activated receptor γ coactivator 1-α (PPQEAEEPSLLKKLLLAPANT; PRGC1), the sample was concentrated to 0.3 mM. The exchange of LBD-bound dex for other ligands was conducted in the absence of stabilizing CHAPS and coactivator peptide. Excess ligand was dissolved in 50 mM tris (pH 9) containing 10% DMSO (to increase ligand solubility), and dex-bound LBD was exchanged twice into this buffer using a PD10 desalting column. Last, the protein was transferred to the aforementioned DMSO-free phosphate buffer containing CHAPS.

NMR resonance assignment

Assignment of the $^1H/^{13}C/^{15}N$ backbone and $^1H/^{13}C$ methionine methyl resonances has been reported previously for GR_{wt} and GR_{F602S} (*23*).

Relaxation dispersion measurements

Transverse relaxation-optimized spectroscopy (TROSY)–based relaxation-compensated ^{15}N CPMG experiments (*25*, *40*, *41*) were implemented using interleaved acquisition of various CPMG frequencies before sampling the indirect ^{15}N dimension. Data were acquired at a temperature of 298 K and static magnetic field strengths of 14.1 and 18.8 T. ^{13}C CPMG experiments on $^{12}C^{\beta}D_2{}^{12}C^{\gamma}D_2{}^{13}CHD_2$ methionine-labeled samples were performed as described (*24*) at a temperature of 298 K. Experiments on GR_{wt} with TIF2 were acquired at static magnetic field strengths of 14.1 and 20.0 T, whereas experiments on GR_{wt} with PRGC1 were acquired at 18.8 T, and experiments on GR_{F602S} with TIF2 were acquired at 14.1 and 18.8 T. Relaxation dispersion data were acquired using a linear two-point approximation of the exponential decay (*42*) at CPMG frequencies (ν_{CP}) of 0 (reference), 67, 100, 133, 200, 267, 300, 333, 400, 500, 600, 800, and 1000 Hz, with duplicates acquired at 0, 200, 400, and 600 Hz. Spectra were processed using Topspin 3.4 (Bruker) and analyzed using NMRView (*43*) or Sparky (*44*). The dependence of the transverse relaxation rate constant (R_2) on ν_{CP} was fitted to a two-state exchange process using MATLAB (MathWorks Inc.) to yield the exchange rate (k_{ex}), as well as the populations (p_i) of the exchanging states and the chemical shift differences (Δδ) between these, as described (*21*, *45*). Error estimates were based on Monte Carlo simulations using 1000 samples (*46*).

Surface plasmon resonance

All SPR measurements were run on Biacore 3000 (GE Healthcare) using as running buffer 10 mM Hepes, 50 mM NaCl, 0.5 mM Tris(2-carboxyethyl)phosphine (TCEP), 0.05% Tween 20 (pH 7.6). To avoid mass transport limitations that may obscure the kinetic analysis/fitting, biotinylated coregulator PRGC1 or TIF2 was immobilized on a two-dimensional carboxylated dextran chip (Xantec) at 270 and 380 response units (RU), respectively, using covalently immobilized NeutrAvidin (2200 RU) as a linker.

GR LBD was incubated with respective ligand at 50 μM and injected for 2 min at 400, 200, and 100 nM in running buffer. After each injection, the surface was regenerated with running buffer supplemented with 0.05% SDS. For all binding curves, the association and dissociation phases were fitted using a typical Langmuir 1:1 interaction model to extract the association (k_{on}) and dissociation rate constant (k_{off}), which was further used to estimate the binding affinity constant according to $K_a = k_{on}/k_{off}$. As a primary validation of the data, the affinities extracted from kinetic fitting were compared with the equilibrium response (i.e., binding coverage) for the different ligands, which were in excellent agreement.

GR reporter gene assay

To identify compounds showing agonist activity at human GR, we used a semi-automated reporter assay based on GRE-*lacZ* transfected ChagGo-K-1 cells. The induction of *lacZ* gene expression through the binding of ligand-bound GR to GRE in the promoter of *lacZ* is measured as the up-regulation of the β-galactosidase activity through a color reaction (change in absorbance).

Stably transfected cryopreserved cells were suspended in RPMI 1640 (Gibco) with 10% fetal bovine serum (Hyclone), 1× nonessential

amino acids (Gibco, 100×), and 1 mM sodium pyruvate (Gibco). The cells were then seeded, 50,000 cells per well in 200 µl in a 96-well plate (Costar 3595), and incubated for 24 hours at 37°C, 5% CO_2, and 95% humidity. Compounds were serially diluted, 1:3 dilutions, to give a 10-point concentration response curve. Compounds and controls were then added to the 96-well cell plate in a volume of 1 µl with a 1 or 0.2 mM start concentration, which gives a final assay start concentration of 5 and 1 µM, respectively. As 100% control, dex was used at a final concentration of 1 µM, and as 0% control, DMSO (0.5%) was used. Incubation at 37°C continued for another 24 hours. Cell medium was removed, and the plate was washed once with phosphate-buffered saline (PBS), and 50 µl of 0.1% Triton X-100 (Chemicon) was added to each well and incubated at room temperature for 20 min, followed by addition of 40 µl of reaction mix per well containing 2.5 mM $MgCl_2$ (Sigma), 0.8% (v/v) β-mercaptoethanol (Sigma), and ortho-nitrophenyl-β-galactoside (2.2 mg/ml; Sigma) in 0.1 M sodium phosphate buffer (pH 7.5), and incubated for 1 hour at 37°C. The reaction was stopped by adding 100 µl per well of stop buffer, 300 mM glycine (Sigma), and 15 mM EDTA (Sigma), pH adjusted to 11.3. Absorbance was measured at 420 nm in PHERAstar Plus3. Raw data output was analyzed in Genedata Screener software, a dose response curve was generated using a four-parameter logistic fit, and the EC_{50} (median effective concentration) values were calculated.

SUPPLEMENTARY MATERIALS

Supplementary material for this article is available at http://advances.sciencemag.org/cgi/content/full/6/29/eabb5277/DC1

View/request a protocol for this paper from *Bio-protocol*.

REFERENCES AND NOTES

1. E. R. Weikum, M. T. Knuesel, E. A. Ortlund, K. R. Yamamoto, Glucocorticoid receptor control of transcription: Precision and plasticity via allostery. *Nat. Rev. Mol. Cell Biol.* **18**, 159–174 (2017).
2. D. W. Cain, J. A. Cidlowski, Specificity and sensitivity of glucocorticoid signaling in health and disease. *Best Pract. Res. Clin. Endocrinol. Metab.* **29**, 545–556 (2015).
3. C. R. Keenan, M. J. Lew, A. G. Stewart, Biased signalling from the glucocorticoid receptor: Renewed opportunity for tailoring glucocorticoid activity. *Biochem. Pharmacol.* **112**, 6–12 (2016).
4. F. Buttgereit, Can we shift the benefit–risk ratio of glucocorticoids? *Lancet Rheumatol.* **2**, E5–E6 (2020).
5. R. K. Bledsoe, V. G. Montana, T. B. Stanley, C. J. Delves, C. J. Apolito, D. D. McKee, T. G. Consler, D. J. Parks, E. L. Stewart, T. M. Willson, M. H. Lambert, J. T. Moore, K. H. Pearce, H. E. Xu, Crystal structure of the glucocorticoid receptor ligand binding domain reveals a novel mode of receptor dimerization and coactivator recognition. *Cell* **110**, 93–105 (2002).
6. K. Edman, A. Hosseini, M. K. Bjursell, A. Aagaard, L. Wissler, A. Gunnarsson, T. Kaminski, C. Köhler, S. Bäckström, T. J. Jensen, A. Cavallin, U. Karlsson, E. Nilsson, D. Lecina, R. Takahashi, C. Grebner, S. Geschwindner, M. Lepistö, A. C. Hogner, V. Guallar, Ligand binding mechanism in steroid receptors: From conserved plasticity to differential evolutionary constraints. *Structure* **23**, 2280–2290 (2015).
7. B. Kauppi, C. Jakob, M. Färnegårdh, J. Yang, H. Ahola, M. Alarcon, K. Calles, O. Engström, J. Harlan, S. Muchmore, A.-K. Ramqvist, S. Thorell, L. Öhmann, J. Greer, J.-Å. Gustafsson, J. Carlstedt-Duke, M. Carlquist, The three-dimensional structures of antagonistic and agonistic forms of the glucocorticoid receptor ligand-binding domain: RU-486 induces a transconformation that leads to active antagonism. *J. Biol. Chem.* **278**, 22748–22754 (2003).
8. D. Ricketson, U. Hostick, L. Fang, K. R. Yamamoto, B. D. Darimont, A conformational switch in the ligand-binding domain regulates the dependence of the glucocorticoid receptor on Hsp90. *J. Mol. Biol.* **368**, 729–741 (2007).
9. A. S. Veleiro, L. D. Alvarez, S. L. Eduardo, G. Burton, Structure of the glucocorticoid receptor, a flexible protein that can adapt to different ligands. *ChemMedChem* **5**, 649–659 (2010).
10. J. K. Lempiäinen, E. A. Niskanen, K.-M. Vuoti, R. E. Lampinen, H. Göös, M. Varjosalo, J. J. Palvimo, Agonist-specific protein interactomes of glucocorticoid and androgen receptor as revealed by proximity mapping. *Mol. Cell. Proteomics* **16**, 1462–1474 (2017).
11. J. Li, J. T. White, H. Saavedra, J. O. Wrabl, H. N. Motlagh, K. Liu, J. Sowers, T. A. Schroer, E. Brad Thompson, V. J. Hilser, Genetically tunable frustration controls allostery in an intrinsically disordered transcription factor. *eLife* **6**, e30688 (2017).
12. J. Milhon, S. Lee, K. Kohli, D. Chen, H. Hong, M. R. Stallcup, Identification of amino acids in the τ2-region of the mouse glucocorticoid receptor that contribute to hormone binding and transcriptional activation. *Mol. Endocrinol.* **11**, 1795–1805 (1997).
13. K. W. Nettles, G. L. Greene, Ligand control of coregulator recruitment to nuclear receptors. *Annu. Rev. Physiol.* **67**, 309–333 (2005).
14. G. A. Schoch, B. D'Arcy, M. Stihle, D. Burger, D. Bär, J. Benz, R. Thoma, A. Ruf, Molecular switch in the glucocorticoid receptor: Active and passive antagonist conformations. *J. Mol. Biol.* **395**, 568–577 (2010).
15. J. A. G. Mackinnon, N. Gallastegui, D. J. Osguthorpe, A. T. Hagler, E. Estébanez-Perpiñá, Allosteric mechanisms of nuclear receptors: Insights from computational simulations. *Mol. Cell. Endocrinol.* **393**, 75–82 (2014).
16. C. D. Okafor, J. K. Colucci, E. A. Ortlund, Ligand-induced allosteric effects governing SR signaling. *Nucl. Receptor Res.* **6**, 1–17 (2019).
17. D. J. Kojetin, T. P. Burris, Small molecule modulation of nuclear receptor conformational dynamics: Implications for function and drug discovery. *Mol. Pharmacol.* **83**, 1–8 (2013).
18. I. M. Chrisman, M. D. Nemetchek, I. M. S. de Vera, J. Shang, Z. Heidari, Y. Long, H. Reyes-Caballero, R. Galindo-Murillo, T. E. Cheatham III, A. L. Blayo, Y. Shin, J. Fuhrmann, P. R. Griffin, T. M. Kamenecka, D. J. Kojetin, T. S. Hughes, Defining a conformational ensemble that directs activation of PPARγ. *Nat. Commun.* **9**, 1794 (2018).
19. R. Brust, J. Shang, J. Fuhrmann, S. A. Mosure, J. Bass, A. Cano, Z. Heidari, I. M. Chrisman, M. D. Nemetchek, A.-L. Blayo, P. R. Griffin, T. M. Kamenecka, T. S. Hughes, D. J. Kojetin, A structural mechanism for directing corepressor-selective inverse agonism of PPARγ. *Nat. Commun.* **9**, 4687 (2018).
20. Z. Heidari, I. M. Chrisman, M. D. Nemetchek, S. J. Novick, A.-L. Blayo, T. Patton, D. E. Mendes, P. Diaz, T. M. Kamenecka, P. R. Griffin, T. S. Hughes, Definition of functionally and structurally distinct repressive states in the nuclear receptor PPARγ. *Nat. Commun.* **10**, 5825 (2019).
21. A. G. Palmer III, C. D. Kroenke, J. P. Loria, Nuclear magnetic resonance methods for quantifying microsecond-to-millisecond motions in biological macromolecules. *Methods Enzymol.* **339**, 204–238 (2001).
22. M. Akke, NMR methods for characterizing microsecond to millisecond dynamics in recognition and catalysis. *Curr. Opin. Struct. Biol.* **12**, 642–647 (2002).
23. C. Köhler, G. Carlström, S. Tångefjord, T. Papavoine, M. Lepistö, K. Edman, M. Akke, Backbone ^{1}H, ^{13}C, and ^{15}N resonance assignments of the ligand binding domain of the human wildtype glucocorticoid receptor and the F602S mutant variant. *Biomol. NMR Assign.* **12**, 263–268 (2018).
24. U. Weininger, Z. Liu, D. D. McIntyre, H. J. Vogel, M. Akke, Specific $^{12}C^{\beta}D_2{}^{12}C^{\gamma}D_2S^{13}C^{\varepsilon}HD_2$ isotopomer labeling of methionine to characterize protein dynamics by ^{1}H and ^{13}C NMR relaxation dispersion. *J. Am. Chem. Soc.* **134**, 18562–18565 (2012).
25. J. P. Loria, M. Rance, A. G. Palmer III, A TROSY CPMG sequence for characterizing chemical exchange in large proteins. *J. Biomol. NMR* **15**, 151–155 (1999).
26. M. D. Heitzer, D. B. DeFranco, Mechanism of action of Hic-5/androgen receptor activator 55, a LIM domain-containing nuclear receptor coactivator. *Mol. Endocrinol.* **20**, 56–64 (2006).
27. R. Chodankar, D.-Y. Wu, B. J. Schiller, K. R. Yamamoto, M. R. Stallcup, Hic-5 is a transcription coregulator that acts before and/or after glucocorticoid receptor genome occupancy in a gene-selective manner. *Proc. Natl. Acad. Sci. U.S.A.* **111**, 4007–4012 (2014).
28. L. Ripa, K. Edman, M. Dearman, G. Edenro, R. Hendrickx, V. Ullah, H.-F. Chang, M. Lepistö, D. Chapman, S. Geschwindner, L. Wissler, P. Svanberg, K. Lawitz, J. Malmberg, A. Nikitidis, R. I. Olsson, J. Bird, A. Llinas, T. Hegelund-Myrbäck, M. Berger, P. Thorne, R. Harrison, C. Köhler, T. Drmota, Discovery of a novel oral glucocorticoid receptor modulator (AZD9567) with improved side effect profile. *J. Med. Chem.* **61**, 1785–1799 (2018).
29. K. Suino-Powell, Y. Xu, C. Zhang, Y.-G. Tao, W. D. Tolbert, S. S. Simons Jr., H. E. Xu, Doubling the size of the glucocorticoid receptor ligand binding pocket by deacylcortivazol. *Mol. Cell. Biol.* **28**, 1915–1923 (2008).
30. S. J. Pfaff, R. J. Fletterick, Hormone binding and co-regulator binding to the glucocorticoid receptor are allosterically coupled. *J. Biol. Chem.* **285**, 15256–15267 (2010).
31. V. J. Hilser, E. B. Thompson, Structural dynamics, intrinsic disorder, and allostery in nuclear receptors as transcription factors. *J. Biol. Chem.* **286**, 39675–39682 (2011).
32. G. Weber, Ligand binding and internal equilibiums in proteins. *Biochemistry* **11**, 864–878 (1972).
33. J. A. Schellman, Macromolecular binding. *Biopolymers* **14**, 999–1018 (1975).
34. H. N. Motlagh, V. J. Hilser, Agonism/antagonism switching in allosteric ensembles. *Proc. Natl. Acad. Sci. U.S.A.* **109**, 4134–4139 (2012).
35. M. J. Garabedian, K. R. Yamamoto, Genetic dissection of the signaling domain of a mammalian steroid receptor in yeast. *Mol. Biol. Cell* **3**, 1245–1257 (1992).
36. A. I. Shulman, C. Larson, D. J. Mangelsdorf, R. Ranganathan, Structural determinants of allosteric ligand activation in RXR heterodimers. *Cell* **116**, 417–429 (2004).

37. K. W. Nettles, J. Sun, J. T. Radek, S. Sheng, A. L. Rodriguez, J. A. Katzenellenbogen, B. S. Katzenellenbogen, G. L. Greene, Allosteric control of ligand selectivity between estrogen receptors α and β: Implications for other nuclear receptors. *Mol. Cell* **13**, 317–327 (2004).
38. T. Hegelund Myrbäck, S. Prothon, K. Edman, J. Leander, M. Hashemi, M. Dearman, G. Edenro, P. Svanberg, E.-M. Andersson, J. Almqvist, C. Ämmälä, R. Hendrickx, Z. Taib, K. A. Johansson, A. R. Berggren, C. M. Keen, U. G. Eriksson, R. Fuhr, B. C. L. Carlsson, Effects of a selective glucocorticoid receptor modulator (AZD9567) versus prednisolone in healthy volunteers: Two phase 1, single-blind, randomised controlled trials. *Lancet Rheumatol.* **2**, E31–E41 (2020).
39. F. W. Studier, Protein production by auto-induction in high-density shaking cultures. *Protein Expr. Purif.* **41**, 207–234 (2005).
40. K. Pervushin, R. Riek, G. Wider, K. Wüthrich, Attenuated T_2 relaxation by mutual cancellation of dipole–dipole coupling and chemical shift anisotropy indicates an avenue to NMR structures of very large biological macromolecules in solution. *Proc. Natl. Acad. Sci. U.S.A.* **94**, 12366–12371 (1997).
41. J. P. Loria, M. Rance, A. G. Palmer, A relaxation-compensated Carr–Purcell–Meiboom–Gill sequence for characterizing chemical exchange by NMR spectroscopy. *J. Am. Chem. Soc.* **121**, 2331–2332 (1999).
42. F. A. A. Mulder, B. Hon, A. Mittermaier, F. W. Dahlquist, L. E. Kay, Slow internal dynamics in proteins: Application of NMR relaxation dispersion spectroscopy to methyl groups in a cavity mutant of T4 lysozyme. *J. Am. Chem. Soc.* **124**, 1443–1451 (2002).
43. B. A. Johnson, R. A. Blevins, NMR View: A computer program for the visualization and analysis of NMR data. *J. Biomol. NMR* **4**, 603–614 (1994).
44. T. D. Goddard, D. G. Kneller, SPARKY 3, University of California, San Francisco (2002).
45. J. P. Carver, R. E. Richards, A general two-site solution for the chemical exchange produced dependence of T_2 upon the Carr-Purcell pulse separation. *J. Magn. Reson.* **6**, 89–105 (1972).
46. W. H. Press, B. P. Flannery, S. A. Teukolsky, W. T. Vetterling, *Numerical Recipes. The Art of Scientific Computing* (Cambridge Univ. Press, 1986).
47. Y. He, W. Yi, K. Suino-Powell, X. E. Zhou, W. D. Tolbert, X. Tang, J. Yang, H. Yang, J. Shi, L. Hou, H. Jiang, K. Melcher, H. E. Xu, Structures and mechanism for the design of highly potent glucocorticoids. *Cell Res.* **24**, 713–726 (2014).

Acknowledgments: We acknowledge NMR measurement time at the Swedish NMR Center located at the University of Gothenburg and Umeå University. We thank J. Uhlander for comments on the manuscript and M. Akke for help with preparing Fig. 6, including statistical analysis. **Funding:** This work was supported by AstraZeneca and the Swedish Research Council (621-2014-5815) awarded to M.A. **Author contributions:** C.K. and S.T. performed protein expression and purification. V.U. performed organic synthesis. U.K. performed biochemical assays. C.K., G.C., U.W., and M.A. performed NMR experiments and analysis. A.G. performed SPR experiments and analysis. G.C. and M.A. performed statistical thermodynamic modeling. G.C., M.L., T.P., K.E., and M.A. performed overall project design. **Competing interests:** S.T., V.U., M.L., A.G., T.P., and K.E. are employed by AstraZeneca or were at the time that this study was conducted. The authors declare that they have no competing interests. **Data and materials availability:** All data needed to evaluate the conclusions in the paper are present in the paper and/or the Supplementary Materials. Additional data related to this paper may be requested from the authors.

Submitted 1 March 2020
Accepted 5 June 2020
Published 17 July 2020
10.1126/sciadv.abb5277

Citation: C. Köhler, G. Carlström, A. Gunnarsson, U. Weininger, S. Tångefjord, V. Ullah, M. Lepistö, U. Karlsson, T. Papavoine, K. Edman, M. Akke, Dynamic allosteric communication pathway directing differential activation of the glucocorticoid receptor. *Sci. Adv.* **6**, eabb5277 (2020).

Dynamic allosteric communication pathway directing differential activation of the glucocorticoid receptor

C. Köhler, G. Carlström, A. Gunnarsson, U. Weininger, S. Tångefjord, V. Ullah, M. Lepistö, U. Karlsson, T. Papavoine, K. Edman and M. Akke

Sci Adv **6** (29), eabb5277.
DOI: 10.1126/sciadv.abb5277